Journal of Molecular Spectroscopy **208,** 101–109 (2001)
doi:10.1006/jmsp.2001.8361, available online at http://www.idealibrary.com on IDEAL®

High-Resolution Infrared and Millimeter-Wave Study of D_3SiF: The Ground and $v_3 = 1$ States of the ^{29}Si and ^{30}Si Species, and the $v_3 = v_6 = 1$ and $v_3 = 2$ States of D_3 ^{28}SiF

N. Ben Sari-Zizi,* H. Najib,*,[1] J. Demaison,† L. Margulès,† Z. Kisiel,†,‡ M. Yu. Tretyakov,†,[2] E. B. MKadmi,§ and H. Bürger§

*Laboratoire de Spectronomie Physique Appliquée, Faculté des Sciences, Université Mohammed V Agdal, BP 1014 Rabat, Morocco; †Laboratoire de Physique des Lasers, Atomes et Molécules, UMR CNRS, Université de Lille 1, F-59655 Villeneuve d'Ascq Cedex, France; ‡Instytut Fizyki PAN, Al. Lotnikow 32/46, 02-668 Warsaw, Poland; and §Anorganische Chemie, FB 9, Universität-Gesamthochschule, D-42097 Wuppertal, Germany

Received February 21, 2001; in revised form April 11, 2001; published online June 6, 2001

The ν_3 band of D_3SiF near 890 cm^{-1} recorded with a resolution of 2.4×10^{-3} cm^{-1} has been explored for the ^{29}Si and ^{30}Si isotopic species. Moreover, the $\nu_3 + \nu_6 - \nu_6$ and $2\nu_3 - \nu_3$ bands for the main ^{28}Si isotopomer have been assigned. For this purpose the $\nu_3 + \nu_6$ and $2\nu_3$ bands at 1435.697 and 1769.531 cm^{-1} have been studied. Ground state parameters of the ^{29}Si and ^{30}Si species have been determined by merging newly measured MMW frequencies and ground state combination differences. In addition, $v_3 = 1$ excited state parameters for these species have been obtained. While for the ^{28}Si species the $v_3 = v_6 = 1$ state is locally perturbed by levels of the $v_2 + v_5 = 2$ polyad, the $v_3 = 2$ state appears to be unperturbed, its parameters being predictable from those of the $v_3 = 1$ state. Anharmonicity constants $x_{33} = -4.1334$ cm^{-1} and $x_{36} = -3.6547$ cm^{-1} have been determined.

1. INTRODUCTION

Silyl fluoride H_3SiF, one of the fundamental silicon derivatives, is a strong absorber in the region of CO_2 laser emissions. It has been successfully used to pump far-infrared emissions (*1, 2*) whose assignment has been recently updated with the help of a detailed high-resolution study of the ν_2/ν_5 infrared (IR) bands (*3*). Likewise, H_3SiF is a potential target for Si isotope separation.

Since the ν_3 band of D_3SiF centered at 889 cm^{-1} extends into the spectral region of CO_2 laser emissions, the energy level structures both of the "cold" band of the dominant ^{28}Si isotopomer (abundance 92.2%) and of the ^{29}Si and ^{30}Si species with an abundance of 4.7 and 3.1%, respectively, are of fundamental interest.

Fundamental bands of the different isotopic varieties are accompanied by hot bands. Those belonging to the ^{28}Si species have at room temperature the following Boltzmann factors (B.f.) (*4*):

$$\begin{aligned} \nu_6 &= 550\ cm^{-1}, \quad \text{B.f. } 0.071, \\ \nu_5 &= 702\ cm^{-1}, \quad \text{B.f. } 0.034, \\ \nu_2 &= 710\ cm^{-1}, \quad \text{B.f. } 0.033, \\ \nu_3 &= 889\ cm^{-1}, \quad \text{B.f. } 0.014. \end{aligned}$$

Since the relative intensities of hot bands of ν_3 with these lower vibrational levels are similar to those of the less abundant isotopic species, it is compulsory to treat hot bands of ν_3 and cold bands of the isotopic varieties together. Whenever feasible information deduced from studies of overtones and combination bands, i.e., $\nu_3 + \nu_6$, $\nu_3 + \nu_5$, $\nu_2 + \nu_3$, and $2\nu_3$, should accompany hot band studies.

We have also been interested for some time in the accurate structure of H_3SiF. Since its determination requires combining isotopic ground state data with vibrational corrections in order to have as many A_e and B_e values as possible available, we focus in the present study our interest on the ground state constants of the ^{29}Si and ^{30}Si species of D_3SiF. For this purpose we combine novel millimeter-wave (MMW) measurements of these less abundant species with ground state combination differences (GSCD) obtained from the analysis of the respective ν_3 bands. We have chosen the ν_3 band for several reasons. First, only the ν_3 and ν_6 bands are isolated, regular, and easy to assign (*5*). Second, the spectrum of the ν_6 band is much denser than that of ν_3 owing to the presence of two strong hot bands ($2\nu_6^\ell - \nu_6$), with $\ell = 0$ and $\ell = \pm 2$. Finally, the ν_3 band spectrum available to us is of higher quality (resolution, signal:noise ratio) than that recorded in the ν_6 region. We are also interested in accurate isotopic shifts and anharmonicity constants. These are related to the harmonic and anharmonic force fields and may be compared with *ab initio* calculations, the most recent ones being those by Thiel *et al.* (*6*).

Experimental work on the rare ^{29}Si and ^{30}Si isotopes of D_3SiF reported in the literature is scarce, while that on the major isotope ^{28}Si is much more extensive and comprises the ground, $v_3 = 1$,

[1] Permanent address: Département de Physique, Faculté des Sciences, Université Ibn Tofaïl, BP 133, Kénitra, Morocco.

[2] Permanent address: Institute of Applied Physics, Nizhnii Novgorod, Russia 603024.

0022-2852/01 $35.00

$v_6 = 1$ and 2 (*5*), and $v_2 = 1/v_5 = 1$ dyad level (*7*) states. The available ground state parameters of D_3 ^{28}SiF include both the "*J*-dependent" coefficients obtained from a merge of rotational data and GSCD (*5*) and the "*K*-dependent" coefficients *A*, D_K, and H_K (*5*) determined by the well-known "loop" method (*8*, *9*). The latter were confirmed by perturbation-allowed lines of the ν_2/ν_5 dyad (*7*).

Isotopic shifts $\Delta\nu(^{28}\text{Si} - ^{29}\text{Si})$ and $\Delta\nu(^{28}\text{Si} - ^{30}\text{Si})$ have been determined from a low-resolution spectrum and the experimental force field (*10*), and a few pure rotational lines with *J* 1–0 and 2–1 of the ^{29}Si and ^{30}Si species have been measured (*11*).

In the present work which extends our previous studies on D_3SiF (*5*, *7*) we report on the ground states of D_3 ^{29}SiF and D_3 ^{30}SiF as determined by a merge of rotational data from the MMW region and GSCD in the ν_3 band, and furthermore the analyses of the $2\nu_3 - \nu_3$ hot and $2\nu_3$ overtone bands. Transitions of the $\nu_3 + \nu_6 - \nu_6$ hot band have been assigned but their fit deemed unnecessary in view of the (though perturbed) much more complete combination band $\nu_3 + \nu_6$ near 1440 cm^{-1}, the investigation of which will be reported in the following, too.

2. EXPERIMENTAL DETAILS

Experimental details are the same as reported (*5*). For convenience major features are repeated here. The sample was synthesized by reacting D_3SiI with SbF_3 in a sealed glass ampoule at room temperature and purified by repeated fractional condensation. The natural Si isotopic abundance in the sample was 92.2% ^{28}Si, 4.7% ^{29}Si, and 3.1% ^{30}Si, and there was ca. 3% HD_2SiF present.

Two IR spectra were recorded in Wuppertal (Germany) with a Bruker 120HR interferometer equipped with a globar source and a KBr beam splitter. The conditions are detailed in Table 1.

TABLE 1
Experimental Details for Infrared Spectra

Spectrum No.	I	II
	ν_3 (889 cm^{-1}) hot bands	$\nu_3 + \nu_6$ (1435 cm^{-1}) $2\nu_3$ (1770 cm^{-1})
Resolution (10^{-3} cm^{-1}) (1/MOPD)[a]	2.4	5.0
Region (cm^{-1})	580-1080	750-2000
No. of scans	350	667
Detector	LN_2 - MCT600	LN_2 - MCT800
Filter	>1200 cm^{-1}	>2000 cm^{-1}
Path length (cm)	28	400
Pressure (Pa)	50	800
Calibration, Region	CO_2 (670 cm^{-1})[b]	H_2O (1450 cm^{-1})[c]
Precision (10^{-3} cm^{-1})[d]	0.1	0.2
Accuracy (10^{-3} cm^{-1}), Ref. (*14*)	(1)	1

[a] Maximum Optical Path Difference.
[b] Ref. (*13*).
[c] Ref. (*13*) with post-calibration (*14*).
[d] Precision of unblended, medium intensity lines.

The MMW measurements of the ground state rotational lines were performed in Lille (France) with a spectrometer (*12*) using a Russian-built backward-wave source emitter in the range 486–680 GHz phase-locked against a MMW frequency synthesizer working in the region 78–118 GHz. The absorption was detected with a LHe-cooled InSb bolometer. The frequency accuracy is estimated better than about 50 kHz.

3. DESCRIPTION OF THE SPECTRA AND ASSIGNMENTS

The tasks of the present study are:

—the analysis of the ν_3 bands belonging to the ^{29}Si and ^{30}Si species in order to determine the ground and $v_3 = 1$ excited state parameters using spectrum I;

—the analysis of the $v_3 = 2$ and $v_3 = v_6 = 1$ states of the parent ^{28}Si isotopic species using the cold $2\nu_3$ and $\nu_3 + \nu_6$ bands from spectrum II jointly with the $2\nu_3 - \nu_3$ and $\nu_3 + \nu_6 - \nu_6$ hot bands from spectrum I.

3.1. *The ν_3 Band Region*

The ν_3 band region, an overview of which is shown in Fig. 1 of Ref. (*5*) while some details are illustrated in Fig. 4 of Ref. (*5*), is dominated by the cold ν_3 band of the ^{28}Si isotope. The accompanying weak bands belonging to the rare isotopes ^{29}Si and ^{30}Si, and the hot bands, are well discernible only in the narrow windows between adjacent *J* clusters of the major species, and as ^QQ branches. The latter are illustrated in Fig. 1. In spite of their limited usefulness for the rotational analyses owing to their density the ^QQ branches nevertheless are valuable pieces of data to locate the band centers. On the basis of their intensities and the predicted shifts from the ν_3 band center of D_3 ^{28}SiF at 888.89 cm^{-1} (denoted (a)) they can be assigned as follows.

The ^QQ branches denoted (b), with a sharp edge at 885.24 cm^{-1}, are assigned to $\nu_3+\nu_6-\nu_6$. The shift of -3.65 cm^{-1} agrees with $x_{36} = -3.73$ cm^{-1} as predicted by *ab initio* calculations (*6*), and the relative intensity corresponds to the prediction (7.1%; see above). Some ^QP clusters are visible at low *J*, Fig. 1.

The ^QQ branches denoted (c), with a high-wavenumber edge at 882.38 cm^{-1}, see Fig. 4 of Ref. (*5*), are assigned to ν_3 of the ^{29}Si species on the basis of the agreement of the intensity relative to ^{28}Si with that expected (4.7% : 0.922 = 5.1%), the shift calculated from an harmonic force field, and the resemblance of the shape of the ^QQ branches (Fig. 4 in (*5*)) with those of feature (a). This latter agreement rules out that (c) belongs to any of the hot bands $\nu_2 + \nu_3 - \nu_2$ or $\nu_3 + \nu_5 - \nu_5$ in spite of their similar intensities because the lower and upper states of the hot bands $\nu_2 + \nu_3 - \nu_2$ and $\nu_3 + \nu_5 - \nu_5$ are involved in strong Coriolis (and other) interactions. Therefore the shapes of the respective ^QQ branches of these hot bands will differ from feature (c) and should appear spread without revealing any sharp high-wavenumber edge. Finally, conceivable hot bands $\nu_3 + 2\nu_6^{\ell} -$

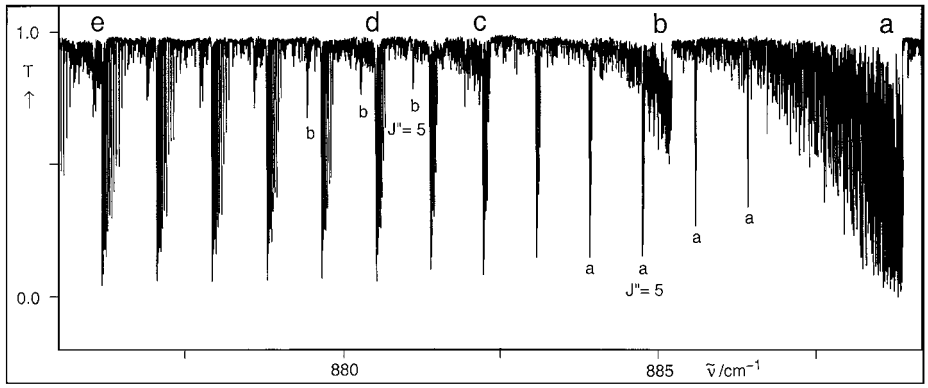

FIG. 1. Survey spectrum of D_3SiF in the ν_3 Q-branch region. The notation of the Q branches and some ^QP clusters is (a) ν_3, ^{28}Si; (b) $\nu_3 + \nu_6 - \nu_6$, ^{28}Si; (c) ν_3, ^{29}Si; (d) $2\nu_3 - \nu_3$, ^{28}Si; and (e) ν_3, ^{30}Si.

$2\nu_6^\ell$, $\ell = 0$ and ± 2, should be weaker and shifted from (a) by about $-7.3\ cm^{-1}$, which is significantly more than that observed for (c), $-6.51\ cm^{-1}$.

The hot band (d) shifted from (a) by $-8.25\ cm^{-1}$ is unambiguously assigned to $2\nu_3 - \nu_3$ because $2\nu_3$ is definitely located at $1759.53\ cm^{-1}$ (see below).

The ^QQ branches denoted (e) belong to ν_3 of $D_3\ ^{30}SiF$. This assignment is supported by the intensity (calc. 3.4% relative to (a)), the shift ($-12.63\ cm^{-1}$), which is about twice that of (c), the shape of the ^QQ branches similar to (a) and (c), and the association with ^QP and ^QR branches on which the analysis is based (see below).

Note that the ^QQ branches (c), (d), and (e) are increasingly overlapped by ^QP clusters of ν_3 and $\nu_3 + \nu_6 - \nu_6$ of the ^{28}Si species, their widths increasing with J. Because of their red shift from ν_3 of $D_3\ ^{28}SiF$, all isotope and hot bands offer favorable conditions for detecting some of the J clusters of the ^QP branches. With consideration of the respective B_0 values their assignment was found by means of ground (lower) state combination differences (GSCD and LSCD, respectively). Figure 2 illustrates J clusters belonging to ^{29}Si and ^{30}Si species which are similar to those of the parent band, while those of the $\nu_3 + \nu_6 - \nu_6$ hot band differ sharply owing to ℓ-doubling and the different nuclear spin statistical weights.

However, the $+\ell$ and $-\ell$ subbands of the $\nu_3 + \nu_6 - \nu_6$ hot band with intensity enhancement of the $K = (3p + 1)$ and $(3p - 1)$ series, respectively, overlap in such a fashion that a misinterpretation is likely to occur. Therefore it was advantageous to compute the positions of individual hot band lines from those of the $\nu_3 + \nu_6$ combination band using lower state energies from Ref. (5).

The $^QP_K(10)$ cluster of the $\nu_3 + \nu_6 - \nu_6$ hot band shown in Fig. 2c is a favorable example. The $\ell = +1$ (top) and $\ell = -1$ (bottom) series are visible at lower energies from the onset of the "cold" ^{28}Si, ν_3 band cluster $^QP_K(14)$. Owing to the A_1A_2 splitting of the $k\ell = 1$ level of ν_6 there are altogether three transitions for $K = 1$.

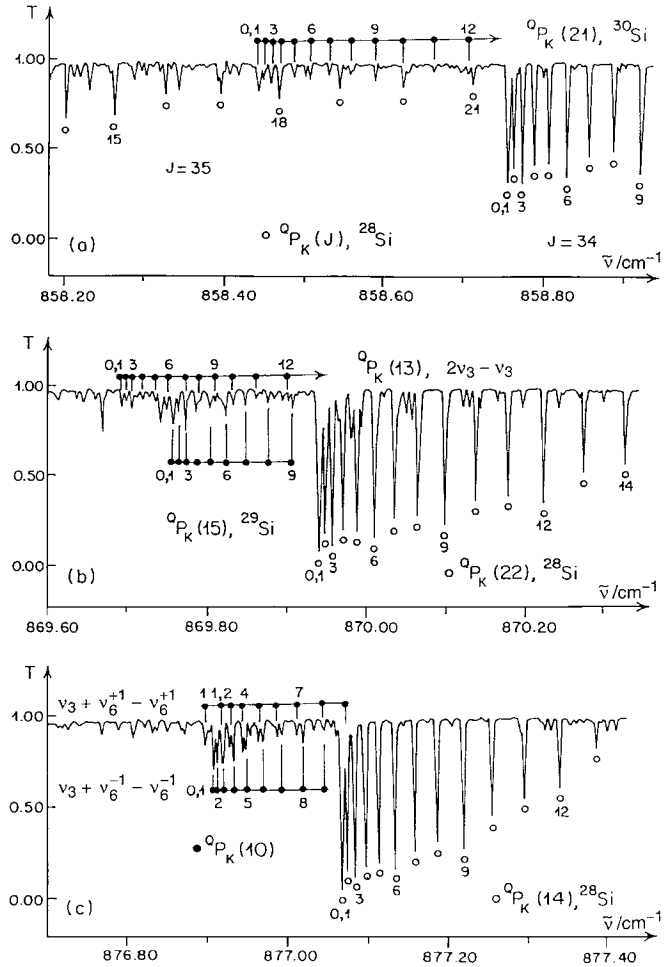

FIG. 2. Some ^QP clusters of the ν_3 band. (a) The $^QP_K(34)$ and $^QP_K(35)$ clusters of ν_3, ^{28}Si, with K labeling below the trace, and the $^QP_K(21)$ cluster of ^{30}Si, with K labeling above the trace. (b) The $^QP_K(22)$ cluster of ν_3, ^{28}Si, and the overlapping clusters $^QP_K(13)$ of $2\nu_3 - \nu_3$, ^{28}Si, and $^QP_K(15)$ of ν_3, ^{29}Si. (c) The $^QP_K(14)$ clusters of ν_3, ^{28}Si, and the $^QP_K(10)$ cluster, $\nu_3 + \nu_6 - \nu_6$, ^{28}Si. The $\ell = +1$ transitions are labeled above the trace, and the $\ell = -1$ transitions, below the trace.

More generally, ^{Q}P and ^{Q}R clusters of the $\nu_3 + \nu_6 - \nu_6$ hot band reveal overlaps of the $+\ell$ and $-\ell$ subseries, and by other bands, to such an extent that we renounced extracting transition wavenumbers from the spectra in view of the significantly better data on the $v_3 = v_6 = 1$ level available from the combination band $\nu_3 + \nu_6$.

3.2. *The $\nu_3 + \nu_6$ Band Region*

The $\nu_3 + \nu_6$ band centered at 1436 cm^{-1} is quite analogous to the ν_6 band (*5*) but there are significant overlaps and perturbations. First, the overtone triad $2\nu_2$, $\nu_2 + \nu_5^{\pm 1}$, and $2\nu_5^{\ell}$, $\ell = 0, \pm 2$, has respective band centers at 1419, 1412, and 1400 cm^{-1}. This triad gives rise to several weak features in the lower wavenumber part of the $\Delta K = -1$ wing, which could not yet be assigned, while in the $\Delta K = +1$ side no such lines occur. Second, there appear numerous perturbations which are most obvious in the Q branches being uniformly J-degraded to small wavenumber. One of these perturbations occurs near $J = 22$ of the $k\ell = 1$ to 9 sublevels, separations between successive Q-branch lines reaching 0.4 cm^{-1} for $^{R}Q_0(22)$ and $^{R}Q_0(23)$. Starting with $^{R}Q_9$ this perturbation vanishes, and ^{R}Q lines could be assigned with the help of ^{R}R lines by means of GSCD with the exception of the $^{R}Q_0$ branch. In this branch the portion of lines which is in essence unperturbed was assigned with the help of the q_6 coupling term (*5*). Figure 3b illustrates the $^{R}Q_{11}$ branch for $12 \le J \le 23$; this Q-branch region overlaps with $^{R}R_K$ lines for $K \le 6$. As observed for ν_6, the $^{R}R_K(J)$ lines are clustered with $J + 2K =$ constant. The $^{R}R_K(J)$, $^{R}R_{K+1}(J + 2)$, ..., clusters, and the ^{R}Q branches, are uniformly J-degraded to small wavenumber contrary to the $^{R}R_K$ branches of ν_6 where a bandhead occurred at $J = 28$; see Fig. 3 of Ref. (*5*).

Also the $^{P}Q_1$ to $^{P}Q_5$ branches reveal resonance repulsion of successive lines but the repulsion is smaller than in the ^{R}Q branches. As an example, the enhanced separation of the $J = 21$ and 22 lines of $^{P}Q_2$ is just twice that of the $J = 22$ and 23 lines, Fig 3a. The $^{P}Q_3$ branch for $3 \le J \le 20$ is displayed in Fig. 3a. We note that $^{P}Q_3$ lines are not split into A_1A_2 doublets up to $J = 26$; such splitting is forecasted for $J \ge 30$. However, no splitting could be detected owing to vanishing intensity and blending of respective transitions. We note that A_1A_2 splitting of $^{P}Q_3$ in ν_6 had been resolved for $J \ge 27$ and was easily followed up to $J = 40$. With the help of GSCD we also located some $^{P}R_K$ series for $K \le 6$; see Fig. 3b.

The $^{P}P_K(J)$ lines occur in two distinct clusters which have $2J + 3K =$ constant, one with K even and the other with K odd. This distribution is very well expressed around $^{P}P_{12}(12)$ and $^{P}P_9(16)$, respectively, and it differs somewhat from that observed in ν_6 where three clusters occurred; see Fig. 2 in Ref. (*5*).

The $\Delta K = +1$ branches of $\nu_3 + \nu_6$ exert higher intensities than the $\Delta K = -1$ series due to intensity perturbation by the $\ell(2, 2)$ resonance. Thus, assignments in the $\Delta K = -1$ part only reached $J''_{\max} = 35$ and $K''_{\max} = 21$ while 40 and 24, respectively, were attained in the $\Delta K = +1$ branch.

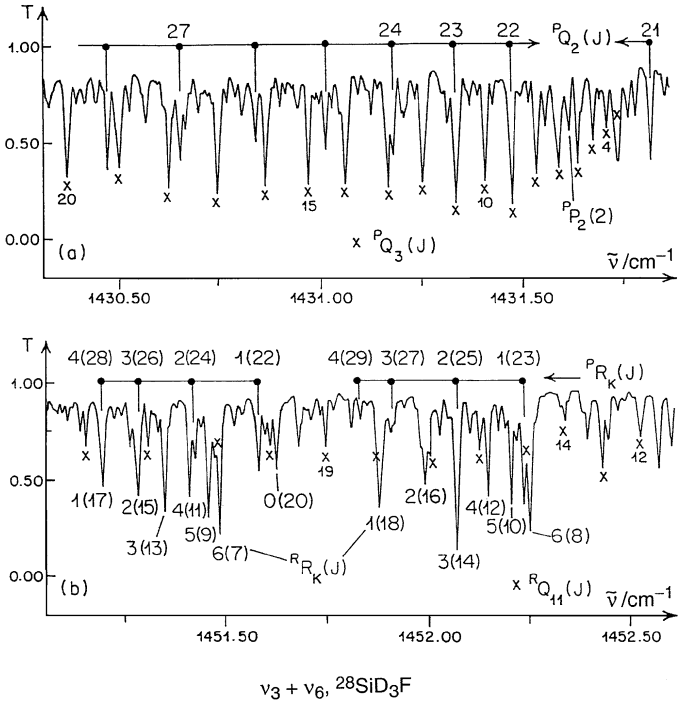

FIG. 3. Two details of the $\nu_3 + \nu_6$ band of D_3SiF. (a) Part of the ^{P}Q-branch region showing the $^{P}Q_2$ branch labeled on top of the trace (note the gap between the $J = 21$ and 22 lines) and the $^{P}Q_3$ branch (denoted $\times$). (b) Part of the $\Delta K = +1$ branch region showing the $^{R}Q_{11}$ branch (denoted $\times$), some $^{P}R_K(J)$ clusters (solid dots and labeled $K''(J'')$ above the trace), and $^{R}R_K(J)$ (labeled $K''(J'')$ below the trace). These belong to the $(J'' + 2K'') = 19$ and 20 manifolds.

3.3. *The $2\nu_3$ Band Region*

The assignment of this textbook example of an unperturbed, resolved parallel band needs no comment; see Fig. 4. The J clusters degrading with K to high wavenumbers are isolated for lower K values but superposition of high-K lines of J clusters with low-K lines of $J + 1$ clusters occurs at higher J, in particular in the denser ^{Q}R branches. Assignments were followed up to $J_{\max} = 56$ and $K_{\max} = 33$, while the respective values for $2\nu_3 - \nu_3$ are only 31 and 18.

4. ANALYSIS AND RESULTS

4.1. *Ground State Constants*

The ground state constants of the major isotopic species $D_3\,^{28}SiF$ have been determined previously by merging pure rotational data and GSCD for the "J-dependent" terms and using the "loop" method for the "K-dependent" terms A, D_K and H_K (*5*). The latter methods provided GSCD with $\Delta K = \pm 3$ from the simultaneous analysis of ν_6, $2\nu_6^{\mp 2}$, and $(2\nu_6^{\pm 2} - \nu_6^{\pm 1})$. This is not feasible for the rare isotopes as long as isotopically

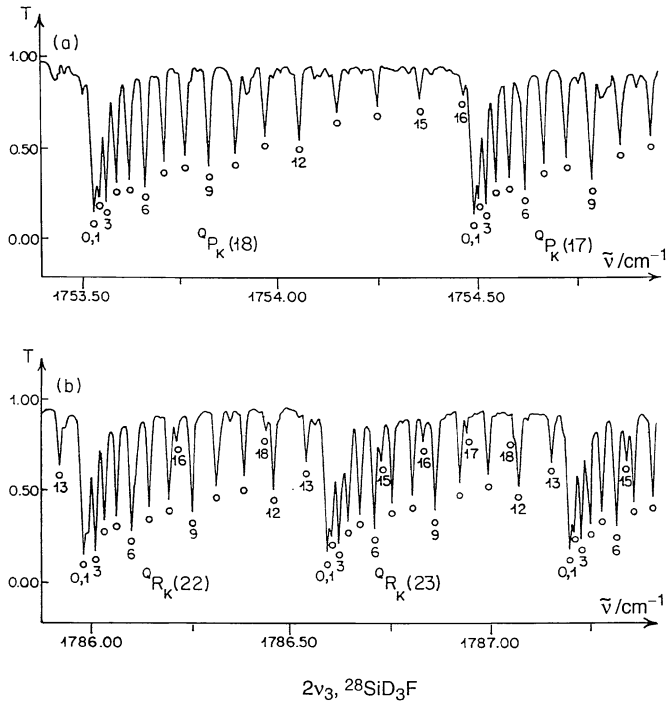

FIG. 4. Part of the $2\nu_3$ band of D_3SiF. (a) $^{Q}P_K(18)$ and low-K part of $^{Q}P_K(17)$ clusters. The K assignment is indicated. (b) $^{Q}R_K(22)$ and $^{Q}R_K(23)$ clusters. The K assignment is given. Note that the $K \geq 14$ lines run into the next higher J cluster.

enriched material is unavailable. So, only the J-dependent parameters could be obtained. For their determination we have both fitted GSCD obtained from ν_3 and merged GSCD and MMW transitions supplemented by three microwave transitions (*11*) for each isotopomer, with all rotational data assigned a relative weight of 1000. We have decided to use the same relative weights for GSCD and MMW data as previously (*5*) although a $1/\sigma^2$ weighting would require an even higher relative weight for the rotational data. The data were fitted to the terms in the energy expression given in Eq. [1] of the Appendix. Programs described in Ref. (*15*) were used. The results for $D_3\ ^{M}SiF$, $M = 28$, 29, and 30, are reported in Table 2, and some statistical data are given.

4.2. The $v_3 = 1$ State Parameters of the ^{29}Si and ^{30}Si Species

These were determined using the ground state parameters reported in Table 2 and including the A_0, $D_{K,0}$, and $H_{K,0}$ values as given for $D_3\ ^{28}SiF$ in Ref. (*5*). Since the ground state parameters were constrained it is more appropriate to report in Table 3 the differences $X_0 - X_3$ rather than the state parameters X_3. Upper state energies were taken as set out in Eq. [2] of the Appendix; sextic centrifugal distortion parameters H_v were constrained to their ground state values H_0. Table 3 reports the results for the $D_3\ ^{M}SiF$ species. While the difference $(A_0 - A_3)$ increases with increasing M, noting that the increase is independent of the chosen A_0 value, $(B_0 - B_3)$ decreases as B decreases. For the ^{29}Si and ^{30}Si species the differences $(D_0 - D_v)$ are just fitting parameters but one should keep in mind that the differences $(D_{J,0} - D_{J,3})$ and $(D_{JK,0} - D_{JK,3})$ are small (<2.5%) with regard to $D_{J,0}$ and $D_{JK,0}$. Larger differences (≤10%) are noted for $(D_{K,0} - D_{K,3})$ but the latter is strongly correlated with $(A_0 - A_3)$.

The superiority of the ^{28}Si data thanks to their higher precision, their greater number, and the availability of MMW data for the $v_3 = 1$ state is evident. The isotopic shifts were

TABLE 2
Ground State Parameters (cm^{-1}) of D_3SiF

	$D_3{}^{28}SiF$, Ref.(5)		$D_3{}^{29}SiF$, this work[a]		$D_3{}^{30}SiF$, this work[a]	
	IR data only	(IR+MMW) data	IR data only	(IR+MMW) data	IR data only	(IR+MMW) data
B_0	0.408 720 775(83)	0.408 720 529(32)	0.406 135 34(54)	0.406 134 47(12)	0.403 679 29(80)	0.403 678 33(18)
$D_{J,0} \times 10^6$	0.358 78(48)	0.358 719(31)	0.354 67(24)	0.354 21(10)	0.350 39(45)	0.349 63(15)
$D_{JK,0} \times 10^6$	4.165 35(56)	4.165 36(17)	4.150 7(55)	4.139 2(12)	4.110 5(89)	4.114 0(25)
$H_{J,0} \times 10^{13}$	1.440(81)	1.349(59)	1.349[b]	1.349[b]	1.349[b]	1.349[b]
$H_{JK,0} \times 10^{11}$	1.506(14)	1.552 1(83)	1.552[b]	1.61(11)	1.552[b]	1.59(20)
$H_{KJ,0} \times 10^{11}$	7.651(71)	7.235(23)	7.235[b]	7.15(14)	7.235[b]	7.17(15)
No. of data	2388	2388 + 59	425	425 + 25	324	324 + 36
J_{max}/K_{max}, IR	61/34	61/34	45/22	45/22	38/13	38/13
J_{max}/K_{max}, MMW		25/24		25/24		25/25
$\sigma \times 10^3$, IR	0.093		0.323		0.363	
$\sigma \times 10^6$, MMW		1.31		0.93		1.01

[a] The K-dependent parameters, not determined for $D_3\ ^{29}SiF$ and $D_3\ ^{30}SiF$, assumed to be equal to those obtained in Ref. (*5*) for $D_3\ ^{28}SiF$, are: $A_0 = 1.424\ 1539(20)\ cm^{-1}$, $D_{K,0} = 2.075(17) \times 10^{-6}\ cm^{-1}$ and $H_{K,0} = -2.05 \times 10^{-10}\ cm^{-1}$.
[b] Constrained to the $D_3\ ^{28}SiF$ value because not determined with significance.

TABLE 3
Parameters (cm^{-1}) of the $v_3 = 1$ State of D_3SiF

	$D_3{}^{28}SiF$, Ref.(5)	$D_3{}^{29}SiF$, this work	$D_3{}^{30}SiF$, this work
ν_0	888.898 812(11)	882.378 162(36)	876.264 046(46)
$(A_0 - A_3) \times 10^4$	3.761 07(99)	3.939 5(75)	4.347(18)
$(B_0 - B_3) \times 10^3$	2.156 461(21)	2.130 98(10)	2.106 36(16)
$(D_{J,0} - D_{J,3}) \times 10^8$	0.811 6(14)	0.888 6(55)	0.857(12)
$(D_{JK,0} - D_{JK,3}) \times 10^8$	-0.130 4(94)	3.329(92)	1.04(17)
$(D_{K,0} - D_{K,3}) \times 10^7$	0.074 5(29)	-2.738(15)	-1.12(14)
$(H_{J,0} - H_{J,3}) \times 10^{13}$	-1.727(26)	0[a]	0[a]
$(H_{JK,0} - H_{JK,3}) \times 10^{11}$	-0.194 6(32)	0[a]	0[a]
$(H_{KJ,0} - H_{KJ,3}) \times 10^{11}$	0[a]	0[a]	0[a]
$(H_{K,0} - H_{K,3}) \times 10^{10}$	-0.79(25)	0[a]	0[a]
No. of data	2240 IR + 38MMW	1032 IR	700 IR
J_{max}/K_{max}	62/31	45/22	38/13
$\sigma \times 10^3$, IR	0.123	0.383	0.352
$\sigma \times 10^6$, MMW	1.16	-	-

[a] Constrained.

accurately determined: $\Delta\nu_3(^{28}Si - {}^{29}Si)$ 6.52065(5) cm^{-1} and $\Delta\nu_3(^{28}Si - {}^{30}Si)$ 12.63477(6) cm^{-1}. We note that these are significantly larger than those for H_3SiF (4.565 and 9.001 cm^{-1}, *16*).

4.3. The $v_3 = v_6 = 1$ State of $D_3{}^{28}SiF$

The apparent differences between the spectra of ν_6 on the one hand and on the other hand of $\nu_3 + \nu_6$, in particular its low-wavenumber portion, imply substantial perturbations of the $v_3 = v_6 = 1$ combination state. The overtones of the Coriolis interacting vibrational dyad ν_2/ν_5 (*7*) give rise to a $(v_2 + v_5) = 2$ triad consisting of a v, ℓ rovibrational hexad. This system of coupled levels whose structure is still obscure can interact with the $v_3 = v_6 = 1$, $\ell = \pm 1$ rovibrational dyad, creating an octad. Fortunately, interactions between the dyad and the hexad, which are quartic, are weak and therefore only local, and a large number of $\nu_3 + \nu_6$ transitions is left which are only weakly or even not affected so that they can be selected for a fit by a quasi-unperturbed model.

Combining experimental ν_2, ν_5 wavenumbers with *ab initio* anharmonicity constants (*6*) the following band centers are predicted:

$$\begin{array}{ll} 2\nu_2 & 1419.0\ cm^{-1} \\ \nu_2 + \nu_5 & 1412.4\ cm^{-1} \\ 2\nu_5,\ \ell = \pm 2 & 1402.9\ cm^{-1} \\ 2\nu_5,\ \ell = 0, & 1400.7\ cm^{-1}. \end{array}$$

The zero-order frequencies of the associated K levels are moreover modulated by the different $A\zeta$ values. We have calculated $J = 0$ energies of relevant v, ℓ, K levels with $(A\zeta)_{3,6} = 0.285\ cm^{-1}$, $(A\zeta)_{2,5} = (A\zeta_{55} = -0.180\ cm^{-1}$ and not taking into account J-dependent resonance effects due to Coriolis, $\ell(2, 2)$ and $\ell(2, -1)$, etc., interactions. These are shown in Fig. 5. We conclude that the following crossings are likely to occur:

—of $(\nu_3 + \nu_6)^{+1}$, K and $2\nu_5^{+2}$, $K + 1$ at about $K = 10$
—of $(\nu_3 + \nu_6)^{-1}$, K and $(2\nu_5)^0$, $K + 1$ at about $K = 26$
—of $(\nu_3 + \nu_6)^{-1}$, K and $(2\nu_2)^0$, $K + 1$ at about $K = 11$
—of $(\nu_3 + \nu_6)^{+1}$, K and $(\nu_2 + \nu_5)^{+1}$, K at $K = 25$.

This implies a particular probability of perturbations of $\nu_3 + \nu_6$ near $K'' = 11$ in the $\Delta K = -1$ side and near $K'' = 10$ on the $\Delta K = +1$ side.

This prediction is consistent with the observations, Section 3. One should keep in mind the wide fluctuation of effective B values dependent on J owing to Coriolis and other interactions within the v, ℓ hexad.

To fit the 2389 observed transitions of which 2240 were unit-weighted we have used the energy expression [3] given in the Appendix. In correspondence to ν_6 (*5*), we have added $\ell(2, 2)$ (q resonance) and $\ell(2, -4)$ (t resonance) interactions, Eqs. [4] and [5], respectively. The $\ell(2, -4)$ parameter accounting for

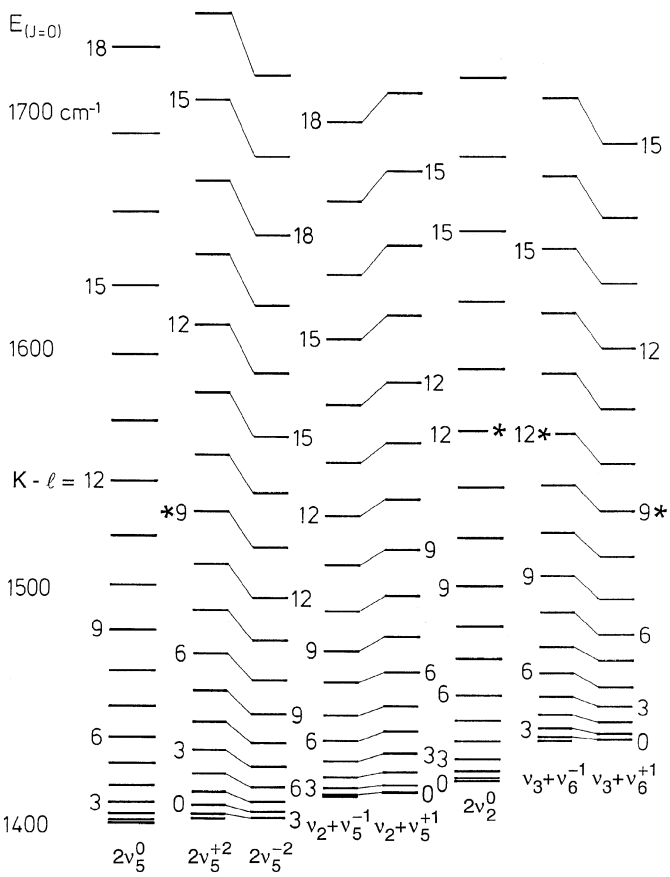

FIG. 5. Upper state $J = 0$ energy levels for $\nu_3 + \nu_6$ and perturbers belonging to the $\nu_2 + \nu_5 = 2$ polyad. Levels are denoted by $(K - \ell)$ labels which are given for A_1A_2 symmetry. Interactions of $\nu_3 + \nu_6$ are likely to come to resonance between sublevels denoted by asterisks.

(unobservable) A_1A_2 splittings of the $k\ell = -2$ sublevel was throughout constrained to the value of the $v_6 = 1$ state (*5*).

A fit of all data, with ground state parameters fixed to the values of Table 2, yielded an unacceptable rms deviation of 29×10^{-3} cm^{-1}, with better average agreement for the (slightly fewer) $\Delta K = -1$ transitions including particular outliers for the $K\Delta K = +9$ and $+10$ subbands (ca. 90×10^{-3} cm^{-1}). Eliminating these subbands from the body of data decreased the rms to ca. 20×10^{-3} cm^{-1}, still indisputable. The residuals were not random, and data blocks with consistently smaller (obs − calc) values were present, while others showed systematic deviations. Removing the systematically shifted transitions whose (obs − calc) values exceeded 3×10^{-3} cm^{-1} left a body of altogether 1354 pieces of data, i.e., ca. 60% of the totally assigned transitions, which could be fitted with $\sigma = 2.17 \times 10^{-3}$ cm^{-1}. This σ value is larger than the precision of the data but smaller than the actual linewidth. The results of this fit are reported in Table 4. With this restricted but significant and representative body of data we ascertained that the $\ell(2, -1)$ resonance is unimportant, as was also found for v_6 (*5*).

Column 2 of Table 4 gives, for comparison, the parameters of the $v_3 = v_6 = 1$ state calculated assuming additivity of the differences between rotational and centrifugal distortion constants for v_3 and v_6 (*5*). The $(A'' - A')$ and $(B'' - B')$ values of both columns are consistent within 5 and 2%, respectively; the $A\zeta^z$ values agree within 0.3% and thus rule out the presence of significant global perturbations.

Moreover, it is pleasing to see that q, η_J, and η_K agree within 4, 0.3, and 10%, respectively. The small $(D'' - D')$ values and higher order η terms are apparently fit parameters which are moreover sensitive to the selection of data included in the fits. From the band centers of v_3, v_6, and $v_3 + v_6$ we determine $x_{36} = -3.6547$ cm^{-1}.

Having analyzed the $v_3 = v_6 = 1$ level we can now better understand the $v_3 + v_6 - v_6$ hot band, Fig. 2c. Even for the unperturbed portion of the hot band there is significant overlap of the $+\ell$ and $-\ell$ components, both being degraded to high wavenumber of the "biparallel" band owing to some v dependence of $A\zeta^z$ (cf. Table 4). Similar observations have been made for $D_3Si^{35}Cl$ (*17*) and $H_3Si^{37}Cl$ (*18*). In view of the superiority of the $v_3 + v_6$ data with regard to those of the $v_3 + v_6 - v_6$ hot band we have desisted from a numerical analysis of the latter data.

TABLE 4
Parameters (cm^{-1}) of the $v_3 = v_6 = 1$ State of D_3 ^{28}SiF

	$v_3 + v_6$	Calculated from v_3 and v_6, Ref. (*5*), assuming additivity
v_0	1435.696 96(14)	1439.351 67
A	1.426 312 5(25)	1.426 214 6
$(A_0 - A_{36}) \times 10^3$	-2.158 6(25)	-2.060 7
B	0.405 347 41(70)	0.405 275 04
$(B_0 - B_{36}) \times 10^3$	3.373 37(70)	3.445 74
$D_J \times 10^6$	0.334 62(66)	0.340 99
$(D_{J,0} - D_{J,36}) \times 10^7$	0.241 6(66)	0.177 9
$D_{JK} \times 10^6$	4.357 5(28)	4.244 2
$(D_{JK,0} - D_{JK,36}) \times 10^7$	-1.922(28)	-0.789
$D_K \times 10^6$	2.067(10)	2.418
$(D_{K,0} - D_{K,36}) \times 10^7$	0.08(10)	-3.43
$A\zeta^z$	0.284 399(93)	0.285 316 1
$\eta_J \times 10^5$	0.698 9(93)	0.701 12
$\eta_K \times 10^5$	2.497(21)	2.819 9
$\eta_{JJ} \times 10^9$	0[a]	0[a]
$\eta_{JK} \times 10^9$	-1.489(80)	0.148 1
$\eta_{KK} \times 10^9$	5.86(49)	2.362
$q \times 10^3$	-1.141 9(28)	-1.102 49
$q_J \times 10^9$	6.469[a]	6.469
$q_K \times 10^6$	6.669(65)	8.904
$t \times 10^9$	5.456[a]	5.456
Total No. of data	2389	-
J_{max}/K_{max}	40/24	
No. of unit-weighted data	1354	
$\sigma \times 10^3$	2.17	-

[a] Constrained as for the $v_6 = 1$ state.
All sextic H terms were constrained to their ground state values.

TABLE 5
Parameters (cm^{-1}) of the $v_3 = 2$ State of D_3 ^{28}SiF

	$2v_3 - v_3$	$2v_3$	Calculated from v_3, Ref. (*5*), assuming additivity
v_0	880.631 777(53)	1769.530 732(25)	1777.797 607
A	1.423 427(3)	1.423 418 3(30)	1.423 401 7
$(A_0 - A_{33}) \times 10^4$	-	7.356(30)	7.522
B	0.404 474 7(3)	0.404 474 53(80)	0.404 407 61
$(B_0 - B_{33}) \times 10^3$	-	4.245 99(80)	4.312 9
$D_J \times 10^6$	0.339 90(34)	0.339 548(95)	0.342 485
$(D_{J,0} - D_{J,33}) \times 10^8$	-	1.923(10)	1.623 2
$D_{JK} \times 10^6$	4.133 5(28)	4.155 04(62)	4.167 95
$(D_{JK,0} - D_{JK,33}) \times 10^8$	-	1.031(62)	-0.260 8
$D_K \times 10^6$	2.067[b]	2.066(26)	2.059
$(D_{K,0} - D_{K,33}) \times 10^8$	-	0.9(26)	1.490
$H_J \times 10^{13}$	3.076[b]	3.34(20)	4.803
$H_{JK} \times 10^{11}$	1.746 7[b]	1.82(10)	1.941
$H_{KJ} \times 10^{11}$	7.235[b]	7.235[a]	7.235[a]
$H_K \times 10^{10}$	-2.04[b]	-2.10(48)	-2.03
No. of data	644	1577	
J_{max}/K_{max}	31/18	56/33	
$\sigma \times 10^3$	0.367	0.249	

[a] Constrained to the ground state value, Ref. (*5*).
[b] Constrained to $v_3 = 1$ state value, Ref. (*5*).

4.4. *The $v_3 = 2$ State of D_3 ^{28}SiF*

The $2v_3 - v_3$ and $2v_3$ data were fitted straightforwardly. The results collected in Table 5 underline the superiority of the $2v_3$ data compared to those of $2v_3 - v_3$, for which in view of the paucity of the data a simpler model was chosen. In consequence the quartic centrifugal distortion constants differ slightly from those of $2v_3$ while the rotational constants are consistent within 3σ. The respective vibrational energies, $880.631777(53) + 888.898812(11) = 1768.530583(64)$

and 1768.530132(11) cm^{-1} differ by 0.15×10^{-3} cm^{-1}, which is significantly less than the accuracy of the data. The anharmonicity constant is $x_{33} = -4.1334$ cm^{-1}. Compared to their extrapolation from ν_3 (*5*), the $(A_0 - A_{33})$ and $(B_0 - B_{33})$ values agree well; the quartic centrifugal distortion constants are in good agreement and the differences $(D_0 - D_{33})$ are small while the sextic centrifugal terms agree within ±30%. The excellent overall consistency of the ν_3 and $2\nu_3$ parameters establishes that the $v_3 = 2$ level is not conceivably perturbed although its location between ν_1 (1578 cm^{-1}) and ν_4 (1615 cm^{-1}) on the one hand and $\nu_2 + 2\nu_6$ (1802 cm^{-1}) and $\nu_5 + 2\nu_6$ (1810 cm^{-1}) on the other might make it suspect of possible perturbations. We note that the experimental anharmonicity constants $x_{33} = -4.1334$ and $x_{36} = -3.6547$ cm^{-1} are in reasonable agreement with their *ab initio* predictions (*6*), −3.44 and −3.73 cm^{-1}, respectively.

5. CONCLUSION

We have analyzed the ν_3 bands of the ^{29}Si and ^{30}Si varieties of D_3SiF present in natural abundance. The "J-dependent" ground state parameters up to sextic centrifugal distortion terms were determined by merging GSCD with respectively 25 and 36 newly measured MMW frequencies with $J \leq 25$; H_J was not determined with significance and therefore constrained to the value of the ^{28}Si isotopomer. Excited state parameters of the $v_3 = 1$ state yielding, among others, accurate isotopic shifts have been determined.

The ν_3 band region was furthermore explored for transitions of the $\nu_3 + \nu_6 - \nu_6$ and $2\nu_3 - \nu_3$ hot bands. These were assigned with the assistance of the concomitantly studied $\nu_3 + \nu_6$ and $2\nu_3$ bands, data of which are much more precise and numerous than those of the hot bands. While the $v_3 = v_6 = 1$ level, although globally not significantly perturbed, is affected by numerous local interactions involving the $(v_2 + v_5) = 2$ polyad, such perturbations are absent in the $v_3 = 2$ state, reliable rotational parameters being predictable from those of the $v_3 = 1$ state. The present study provides accurate wavenumbers for transitions of the rare isotopic species in the 11-μm spectral range that may be pumped by CO_2 laser lines. Moreover, information on the $v_3 = 2$ and $v_3 = v_6 = 1$ states is valuable for ongoing work on the $v_1 = 1/v_4 = 1$ and $(v_2 + v_5) = 2$ polyads.

APPENDIX

Diagonal and Off-Diagonal Matrix Elements of the Hamiltonian Operator

1. Diagonal Matrix Elements

Ground state energies were calculated using the formula

$$\begin{aligned} E(J,K) = {} & B_0 J(J+1) + (A_0 - B_0)K^2 - D_{J,0}J^2(J+1)^2 \\ & - D_{JK,0}J(J+1)K^2 - D_{K,0}K^4 \\ & + H_{J,0}J^3(J+1)^3 + H_{JK,0}J^2(J+1)^2K^2 \\ & + H_{KJ,0}J(J+1)K^4 + H_{K,0}K^6, \end{aligned} \quad [1]$$

where $K = |k|$.

Energies of A_1 vibrational states $(\nu_3, 2\nu_3)$ were computed according to the formula

$$\begin{aligned} E(v_s, J, K) = {} & \nu_{s,0} + (A_s - B_s)K^2 + B_s J(J+1) \\ & - D_{J,s}J^2(J+1)^2 - D_{JK,s}J(J+1)K^2 - D_{K,s}K^4 \\ & + H_{J,s}J^3(J+1)^3 + H_{JK,s}J^2(J+1)^2K^2 \\ & + H_{KJ,s}J(J+1)K^4 + H_{K,s}K^6. \end{aligned} \quad [2]$$

Energies of E vibrational states $(\nu_3 + \nu_6)^{\pm 1}$ were taken as

$$\begin{aligned} E(v, \ell_t; J, k) = {} & \nu_{t,0} + (A_t - B_t)K^2 + B_t J(J+1) \\ & - D_{J,t}J^2(J+1)^2 - D_{JK,t}J(J+1)K^2 - D_{K,t}K^4 \\ & + H_{J,t}J^3(J+1)^3 + H_{JK,t}J^2(J+1)^2K^2 \\ & + H_{KJ,t}J(J+1)K^4 + H_{K,t}K^6 - \left[2A\zeta_t^z \right. \\ & - \eta_{J,t}J(J+1) - \eta_{K,t}K^2 - \eta_{JJ,t}J^2(J+1)^2 \\ & \left. - \eta_{JK,t}J(J+1)K^2 - \eta_{KK,t}K^4\right]k\ell_t. \end{aligned} \quad [3]$$

2. Off-Diagonal Matrix Elements

The $\ell(2, 2)$ interaction (q_t resonance) within $\nu_6^{\pm 1}$ or $(\nu_3 + \nu_6)^{\pm 1}$ was treated by taking the following matrix elements:

$$\begin{aligned} & \langle v_t, \ell_t; J, k|\mathbf{H}/hc|v_t, \ell_t \pm 2; J, k \pm 2\rangle \\ & \quad = -1/4\{q_t + q_{J,t}J(J+1) + q_{K,t}[k^2 + (k \pm 2)^2]\} \\ & \qquad \times [(v_t \pm \ell_t + 2)(v_t \mp \ell_t)]^{1/2}F^{\pm}(J,k)F^{\pm}(J,k+1) \end{aligned} \quad [4]$$

with $F^{\pm}(J,k) = [J(J+1) - k(k \pm 1)]^{1/2}$.

The $\ell(2, -4)$ interaction (t_t resonance) related to the splitting of the $k\ell = -2$ sublevel of $\nu_6^{\pm 1}$ or $(\nu_3 + \nu_6)^{\pm 1}$ had the following matrix element:

$$\begin{aligned} & \langle v_t = 1, \ell_t = -1; J, k+4|\mathbf{H}/hc|v_t = 1, \ell_t = +1; J, k\rangle \\ & \quad = 1/2t_t F(J,k)F(J,k+1)F(J,k+2)F(J,k+3), \end{aligned} \quad [5]$$

with $F(J,k) = [J(J+1) - k(K+1)]^{1/2}$.

ACKNOWLEDGMENTS

The Moroccan CNR is thanked for support of the PARS "Physique25" project, and the Deutsche Forschungsgemeinschaft for a research grant. Professor L. Halonen is thanked for kindly providing the program SYMTOP.

REFERENCES

1 P. B. Davies and D. P. Stern, *Int. J. Infrared Millimeter Waves* **3,** 909–916 (1982).

2 P. B. Davies, A. H. Ferguson, and D. P. Stern, *Infrared Phys.* **25,** 87–90 (1985).

3 D. Papoušek, H. Bürger, A. Rahner, P. Schulz, H. Hollenstein, and M. Quack, *J. Mol. Spectrosc.* **195,** 263–280 (1999).

4 G. Graner, *J. Mol. Spectrosc.* **161,** 58–79 (1993).

5 N. Ben Sari-Zizi, H. Najib, H. Bürger, E. B. MKadmi, Z. Kisiel, M. Yu. Tretyakov, J. Demaison, L. Margulès, and P. Pracna, *J. Mol. Spectrosc.* **197,** 85–99 (1999).

6 W. Thiel, Y. Yamaguchi, and H. F. Schaefer, *J. Mol. Spectrosc.* **132,** 193–206 (1988).

7 M. Badaoui, N. Ben Sari-Zizi, G. Graner, E. B. MKadmi, H. Bürger, and P. Pracna, *J. Mol. Spectrosc.* **200,** 72–88 (2000).

8 G. Graner and H. Bürger, *in* "Vibration–Rotational Spectroscopy and Molecular Dynamics. Advances in Quantum Chemical and Spectroscopical Studies of Molecular Structures and Dynamics" (D. Papoušek, Ed.), pp. 239–297, World Scientific, Singapore, 1997.

9 A. Ceausu, G. Graner, H. Bürger, and P. Pracna, *J. Mol. Spectrosc.* **182,** 218–220 (1997).

10 A. G. Robiette, G. J. Cartwright, A. R. Hoy, and I. M. Mills, *Mol. Phys.* **3,** 541–553 (1971).

11 C. Georghiou, J. G. Baker, and S. R. Jones, *J. Mol. Spectrosc.* **63,** 89–97 (1976).

12 S. Bailleux, M. Bogey, H. Bolvin, S. Civis, M. Cordonnier, A. F. Krupnov, M. Yu. Tretyakov, A. Walters, and L. H. Coudert, *J. Mol. Spectrosc.* **190,** 130–139 (1998).

13 G. Guelachvili and K. Narahari Rao, "Handbook of Infrared Standards," Academic Press, San Diego, CA, 1986.

14 G. Guelachvili and 23 other authors, *Pure Appl. Chem.* **68,** 193–208 (1996).

15 G. L. Caldow, L. O. Halonen, and J. Kauppinen, *Chem. Phys. Lett.* **101,** 100–105 (1983); G. L. Caldow and L. O. Halonen, *Mol. Phys.* **46,** 223–237 (1982).

16 H. Bürger, M. Litz, A. Ceausu, and G. Graner, *J. Mol. Spectrosc.* **182,** 218–220 (1997).

17 A. Ceausu, G. Graner, H. Bürger, E. B. MKadmi, and P. Pracna, *J. Mol. Spectrosc.* **194,** 128–141 (1999).

18 H. Bürger, S. Bailleux, G. Graner, S. Bosc, and Y. Hennequin, *J. Mol. Spectrosc.* **196,** 296–318 (1999).